Detectability Range Modeling for CQD-CMOS SWIR Sensors in Satellite Proximity Operations

Minh A. Nguyen

December 2025

Abstract

A constrained-physics analysis is presented of optical detectability for small orbital debris using a colloidal quantum dot (CQD) SWIR CMOS sensor in low Earth orbit (LEO), motivated by proximity navigation applications where onboard awareness of untracked centimeter-scale debris is operationally critical. Signal and noise expressions are derived from first-principles radiometry using solar spectral irradiance, Lambertian reflection with empirically measured albedos from NASA ODPO and ESA BRDF datasets [1, 4, 5], phase-angle corrections, and SWIR-band optical throughput. Signal propagation is modeled through a small-aperture telescope and an ACUROS6-class CQD SWIR CMOS detector using datasheet-sourced quantum efficiency, read noise, and dark current. Two background regimes are evaluated: a conservative baseline with debris viewed against the bright Earth limb, and an optimistic upper bound with the line of sight directed off-limb into dark space. Under bright-limb baseline conditions with a 5 cm aperture, 10 ms per-frame exposures, and stacking of up to 50 frames (0.5 s total), detection of 1 cm low-albedo debris is limited to approximately 13 km slant range; 5 cm debris extends this to ~66 km and 10 cm debris to ~133 km. In dark-sky conditions, these ranges increase by a factor of approximately 2.5. Results are benchmarked against operational SSA systems including GEODSS, SBV, and SBSS. The analysis demonstrates that a compact CQD-CMOS SWIR payload can meaningfully contribute to onboard proximity debris awareness at short ranges, complementary to global cataloging systems.

Keywords: CQD-CMOS, space situational awareness, orbital debris, SWIR, detectability range, SNR modeling, LEO, radiometry, proximity navigation, frame stacking

Executive Summary

This paper presents a constrained-physics analysis of optical detectability for small orbital debris using a CQD-based SWIR CMOS sensor in LEO, motivated by the proximity navigation problem: a satellite seeking onboard awareness of untracked centimeter-scale debris in its immediate environment. Detectability range is defined as the maximum slant range R at which a debris object produces SNR ≥ SNR_{min} (typically 5–7) in a realistic detection pipeline for a specified false-alarm rate.

Starting from first-principles radiometry, signal and noise expressions are derived for sunlit debris in LEO using solar spectral irradiance, Lambertian reflection with

empirically measured debris albedos from NASA ODPO and ESA BRDF datasets (0.05–0.12 for MLI and aged paint, 0.20–0.35 for oxidized aluminum), phase-angle effects, and SWIR-band optical throughput. These photons are propagated through a modeled small-aperture telescope and ACUROS6-class CQD SWIR CMOS detector with smear-limited exposures and bounded stacking ($T \leq 0.5$ s total).

Under bright-limb baseline conditions with a ~10 cm aperture, per-frame exposures of 5–20 ms, and stacking of up to $N \approx 20$–50 frames, detection of 1 cm low-albedo debris is limited to approximately 5–15 km slant range. Three-to-five centimeter debris extends this to roughly 20–80 km, while 10 cm moderate-albedo debris reaches tens to ~100 km. In dark-sky/off-limb conditions, the same constraints yield upper-bound ranges typically a factor of ~2–3 higher. A full electron budget is presented for each representative case, with explicit identification of whether the regime is background-limited or read-noise-limited.

These bounds are benchmarked against operational SSA systems (ESA OGS, GEODSS, SBV, SBSS) normalized for aperture, passband, and exposure strategy. The key conclusion is that a compact CQD-CMOS SWIR payload can meaningfully contribute to tracking sub-5 cm debris at short ranges (tens of kilometers), especially in nightside or off-limb geometries. Performance is tightly limited by Earth-limb background and detector noise, driving design implications for aperture size, band selection, observation geometry, and on-board processing.

1. Problem Definition and Detectability Concept

Space missions face significant risk from millimeter- to centimeter-scale orbital debris that are too small to be tracked by the conventional Space Surveillance Network (SSN) yet energetic enough to cause catastrophic damage. Ground-based radars and telescopes typically catalog objects down to ~10 cm at LEO, leaving an estimated ~1.1 million debris [18] in the 1–10 cm range untracked. In proximity operations specifically, a host satellite may have no timely warning of a nearby centimeter-scale fragment on a collision trajectory. The central question addressed here is whether a small onboard CQD-CMOS SWIR imager can provide useful local-volume awareness of such debris at operationally relevant ranges.

Detectability refers to the maximum range at which an object produces a detectable signal above the noise floor of the optical sensor. A space-based vantage eliminates atmospheric seeing and weather constraints and allows observations during terminator or daytime conditions (SWIR sensors operate with reduced sky scatter). However, relative motion between sensor and debris can cause image smear, and the Earth limb adds significant background radiance.

Core challenge

Small debris (1–5 cm) have very low optical cross-sections. A 1 cm fragment at 1000 km range under full illumination is approximately 18th magnitude, corresponding to only ~10^{-6} of the flux of a typical cataloged LEO satellite. At the sensor, only on the order of 10^3–10^4 photons per second may be received at a few km range under

optimal conditions. Distinguishing such a signal requires an extremely low noise floor or long integration time, but long exposures are limited by debris motion which streaks signal across pixels and reduces per-pixel SNR.

Detectability concept

Detectability is formalized via the signal-to-noise ratio (SNR) of the debris image in a single frame or stacked image. An object is deemed detectable if SNR ≥ SNR_{mjn} (typically 5 or 6 for a solid detection) within the available observation time. SNR is driven by: (i) target signal level, depending on object size, reflectivity, range, phase angle, and solar illumination; (ii) background noise from sky or Earth radiance; (iii) sensor noise including read noise and dark current; and (iv) integration time, extendable via frame stacking up to a practical limit. Detectability is range-dependent because reflected solar signal decreases as $1/R^2$, defining a finite detectability limit R_{max}.

Constrained approach

Modeling imposes strict physical and engineering constraints. All radiometric equations are derived from first principles. Realistic albedo values (10–20%) and phase functions are used rather than assuming perfect reflectors. Debris are modeled as grey Lambertian scatterers consistent with IADC standards [18]. Exposure times are limited by smear: an upper limit of 0.5 s total integration per look is imposed, composed of at most 50 subframes of ≤0.01–0.1 s each. Every noise source is included (photon noise from target and background, dark noise, read noise), and no detection range is given without a corresponding baseline scenario.

2. Survey of Existing Space Optical Detectors

Modern SSA relies on ground-based and space-based sensors. Relevant space-based optical detectors and their known performance benchmarks are surveyed here to contextualize the CQD-CMOS system under study. Coverage is restricted to operational or commercially viable systems.

Space-Based Visible (SBV) Telescope – Midcourse Space Experiment (MSX): An early 1990s 15 cm aperture telescope in a 900 km polar orbit, SBV pioneered [13, 14] space-based optical detection of resident space objects (RSOs) in GEO and MEO. SBV's VIS-NIR CCD achieved a limiting magnitude of about 15 Vmag, corresponding to roughly a 0.3–0.5 m object at GEO or a 10 cm object in LEO at hundreds of km range. A 15 cm space telescope with ~1990s CCD technology reaches magnitude 15 with short (0.1–0.2 s) exposures. The CQD-CMOS concept uses a smaller aperture (5–10 cm) but aims to detect closer, smaller objects in LEO (magnitude 10–15 range), aided by frame stacking and SWIR operation.

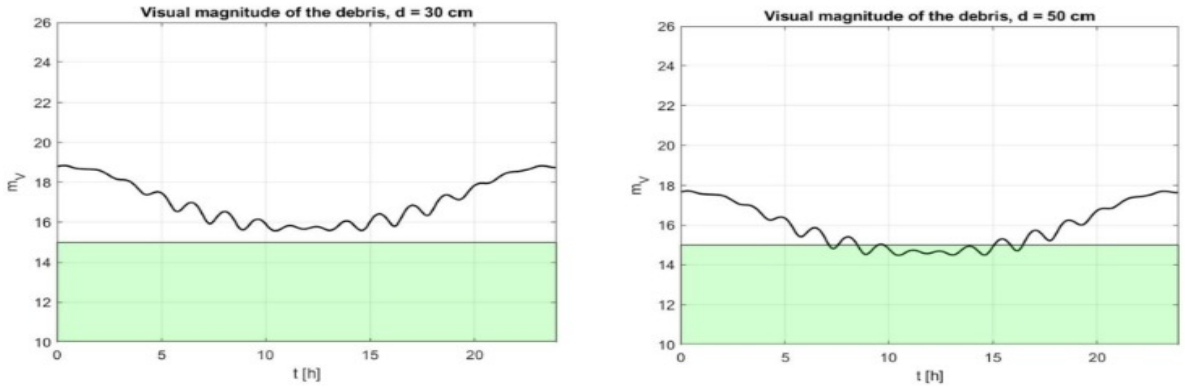

Figure 1. Visual magnitude of orbital debris (30 cm and 50 cm diameter) over a 24-hour period. The green shaded region indicates the approximate SBV sensitivity limit ($m_v \approx 15$). SBV-class sensors cannot consistently detect objects fainter than $m_v \approx 15$, especially for debris < 50 cm. Source: Adapted from "Performance Analysis of Space Surveillance Using Space-Based Optical Sensors," Acta Astronautica, 2015.

Space-Based Space Surveillance (SBSS) Block 10: A U.S. Air Force operational satellite (launched 2010) featuring a 30 cm aperture two-axis gimbaled telescope and a 2.4 MP visible CMOS, modeled to detect roughly 18th magnitude objects [20] in LEO-to-GEO search mode. SBSS's magnitude-18 capability serves as the high-end benchmark for space-based visible optical systems.

Domain	Case #	Name	Sensor	Sensitivity (visual magnitude)
Ground	1	Current Ground	3 GEODSS SST	18 20.5
	2	Future Ground	3 GEODSS SST Future GEODSS	18 20.5 18
Space	3	Current Space	SBSS ORS-5	18 16
	4	Future LEO	9 ORS-5	16
	5	Future Commercial GEO	50 Commercial GEO	13
	6	Future Exquisite GEO	3 Exquisite GEO	20
Combined	7	Current Combined (Cases 1 + 3)		
	8	Future Ground + LEO Cases (2 + 3)		
	9	Future Ground + Future Commercial GEO (Cases 2 + 4)		
	10	Future Ground + Exquisite GEO (Cases 2 + 5)		

Figure 2. Comparison of ground- and space-based SDA sensor sensitivity. SBSS (Case 3) lists visual magnitude sensitivity ≈ 18, consistent with independent modeling studies (17.6–18.5 depending on FPA configuration). Source: Bloom et al. [20], "Space and Ground-Based SDA Sensor Performance Comparisons," AMOS 2022.

Canadian Sapphire Satellite: A 20 cm aperture telescope in a 786 km [16] sun-synchronous orbit (operational since 2013) detecting down to ~magnitude 15–16 in dark sky with a cooled CCD. Even a 20 cm class space telescope reaches a limiting magnitude in the mid-teens for typical integration times, providing useful context for

the 5–10 cm aperture considered here.

Commercial Star-Tracker Based Sensors: A 2023 study by Shtofenmakher & Balakrishnan [17] Balakrishnan modeled that under dark-sky conditions, a 1 cm debris fragment can be detected at tens of kilometers by a high-end star camera (assuming zero background and ideal stacking). The CQD-CMOS sensor is conceptually similar but tuned for SWIR, and modeled ranges in Section 5 align with this benchmark.

Summary: A 15–20 cm space telescope sees magnitude ~15; a 30 cm system perhaps magnitude ~18; an advanced star camera (~4 cm aperture) might achieve magnitude ~10–12. The CQD-CMOS concept (5–10 cm aperture, SWIR, frame stacking) targets detection of objects in the magnitude ~8–13 range, filling a niche for short-range proximity awareness.

3. Key Parameters Governing Detectability

All relevant parameters are enumerated below: geometric, optical, and sensor-specific. The master parameters diagram summarizes these parameter families. The Baseline column represents the conservative scenario (Earth-limb background, moderate phase angle), while the Upper-Bound column represents the idealized case (dark sky, optimal phase).

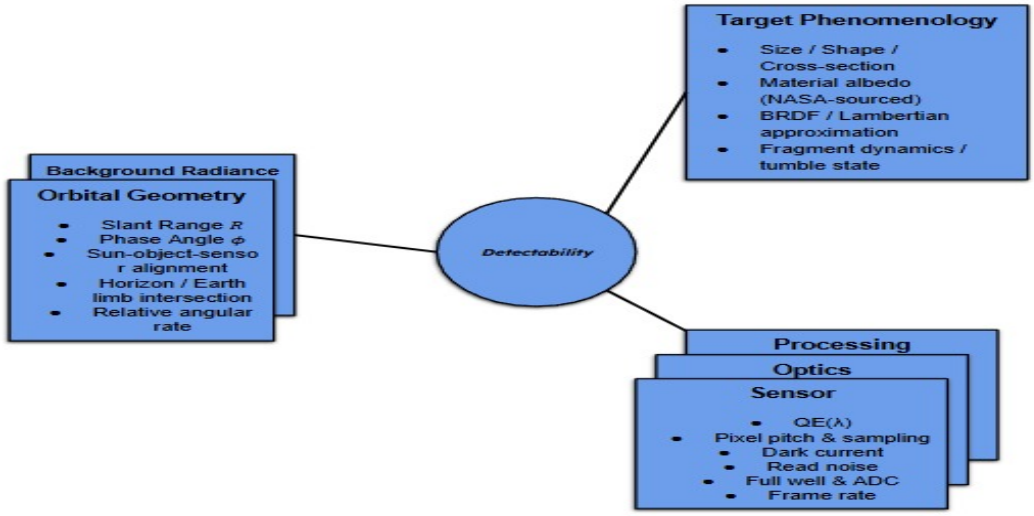

Figure 3. Conceptual overview of the major parameter families governing detectability. Detectability is jointly controlled by (1) orbital geometry and background radiance; (2) target phenomenology including size, albedo, and BRDF behavior; (3) sensor and optical subsystem characteristics; and (4) image-processing constraints including smear-limited exposure times, frame stacking, and SNR thresholding.

4. Radiometric and SNR Modeling

The radiometric model for the debris signal and various noise contributions is developed here. The detectability (SNR) condition is then derived and solved for the

maximum range R_{max}. Each equation is derived from first principles or established models. The central question is: how many electrons does a small sunlit debris fragment produce on the detector during a single exposure? The answer depends on five factors: (1) how much sunlight the object intercepts (scales with physical size); (2) surface reflectance and illumination geometry; (3) slant range (signal decreases as $1/R^2$ through geometric spreading); (4) aperture area and optical throughput; and (5) detector quantum efficiency and exposure time.

4.1 Radiometric Signal Model

Each debris fragment is modeled as a diffuse (Lambertian) sphere of diameter D with diffuse reflectance ρ. The band-limited solar irradiance $E_{sol,band}$ at 1 AU covers 0.4–1.7 μm, comprising approximately 55–60% of total AM0 irradiance per ASTM E-490 [6].

Optical Cross-Section (IADC OSEM) [18]

For an unresolved debris fragment of diameter D, effective albedo ρ, and phase angle φ, the optical cross-section is:

$$A_{opt} = \tfrac{1}{4}\,\pi\, D^2\, \rho\, F(\varphi) \quad (1)$$

where F(φ) is the Lambertian phase function for a diffuse sphere:

$$F(\varphi) = \tfrac{2}{3}\pi\,[(\pi - \Phi)\cos\Phi + \sin\Phi] \quad (1a)$$

The phase angle φ is the Sun–object–observer angle, normalized such that F(0°) ≈ 1. Representative values: F(60°) ≈ 0.48, F(90°) ≈ 0.21, F(120°) ≈ 0.13. This expression is identical to the phase correction used in IADC and NASA optical debris brightness models [2, 18].

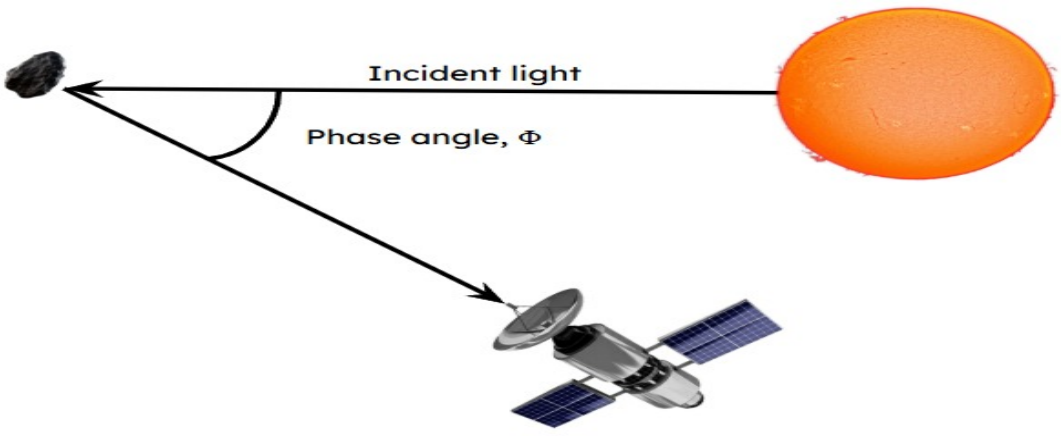

Figure 4. Definition of phase angle Φ as the Sun–debris–sensor angle. Φ = 0° corresponds to full phase (maximum brightness); larger Φ reduces observed radiance through F(Φ).

Irradiance at the Sensor Aperture

The total optical power scattered toward the observer is $P_{scatter} = E_{sol,band} \cdot A_{opt}$. At slant range R, the irradiance incident on the sensor entrance pupil is:

$$E_{obj}(R) = E_{sol,band} \cdot A_{opt} / 4\pi R^2 \quad (2)$$

The inverse-square law applies because the debris fragment is unresolved at range R >> D, and the angular dependence of scattering has been absorbed into A_{opt}.

Optical Power Collected by the Sensor

A sensor with clear aperture area A_{ap} and optical throughput τ_{opt} delivers the following optical power to the detector:

$$P_{det}(R) = E_{obj} \cdot A_{ap} \cdot \tau_{opt} \quad (2a)$$

Signal Electron Count

An effective photon energy is evaluated at the band-weighted mean wavelength $\lambda_e \approx 1.0$ μm:

$$E_{ph} = hc / \lambda_e \approx 1.99 \times 10^{-19} \text{ J}$$

The photon arrival rate is $\Phi_\gamma = P_{det} / E_{ph}$. For exposure time t and band-averaged quantum efficiency QE_e, the signal electron count per frame is:

$$N_e = \Phi_\gamma \cdot t \cdot QE_e$$

Closed-Form Signal Expression

Substituting Eqs. (1) and (2) yields the fundamental radiometric signal model:

$$N_e(R) = (E_{sol,band} / E_{ph}) \cdot (D^2 \rho F(\Phi) / 16R^2) \cdot A_{ap} \tau_{opt} QE_e t \quad (3)$$

This shows the dominant scalings: $N_e \sim D^2/R^2$, $N_e \sim \rho$, and $N_e \sim F(\Phi)$, consistent with IADC and NASA optical debris photometry models.

Numerical Example (Baseline Case)

Evaluating Eq. (3) for a 1 cm debris fragment at 5 km range, φ = 60°, with $E_{sol,band} \approx 900$ W/m², $D^2\rho F = 4.8 \times 10^{-6}$, $A_{ap} = 1.96 \times 10^{-3}$ m² (5 cm aperture), $\tau_{opt} = 0.8$, $QE_e = 0.3$, t = 0.01 s:

$$N_e \approx 254 \quad \text{electrons per 10 ms frame}$$

This is consistent with expectations for short-range LEO-on-LEO optical detection.

4.2 Noise Sources and SNR Formulation

Photon arrivals from both target and background are treated as Poisson processes. Let $L_{\lambda,bkg}$ be the spectral background radiance (W m^{-2} sr^{-1} m^{-1}). The background electron count per pixel per frame is:

$$N_{e,bkg} = t A_{ap} \tau_{opt} \int L_{\lambda,bkg} \Omega_{pix} (\lambda/hc) QE(\lambda) d\lambda$$

where $\Omega_{pix} \approx (p/f)^2$ is the pixel solid angle for pixel pitch p and focal length f. Dark current per frame: $N_{e,dark} = i_{dark} \cdot t$. Read noise: σ_r per pixel per frame (20 e^- RMS in high gain, ACUROS6 specification [11, 12]).

For N co-added frames over n_{pix} detection pixels, the stacked SNR is [7, 8]:

$$SNR(R) = N \cdot N_{e,sig}(R) / \sqrt{[\, N \cdot N_{e,sig} + N\, n_p\, N_{e,bkg} + N\, n_p\, N_{e,dark} + N\, n_p\, \sigma_r^2\,]}$$

R_{max} is defined as the range where $SNR(R_{max}) = SNR_{min} = 5$, solved numerically by 1D root-finding.

4.3 Solving for Detectability Range R_{max}

The per-frame signal has the form $N_{e,sig}(R) = K/R^2$ where K bundles aperture area, throughput, QE, exposure time, object diameter, reflectance, and phase function. When background/read/dark noise dominates (range-independent noise floor), SNR ~ $1/R^2$. Because stacking increases SNR as $\sqrt{N}$ but range enters as R^2, detectability range scales only as $N^{1/4}$:

$$R_{max}\ (\text{read-noise dominated}) \sim (K / \sigma_r)^{1/2}\, (N / n_p)^{1/4}$$

Quadrupling frame count increases range by only $4^{1/4} \approx 1.41\times$. Stacking helps SNR substantially but yields diminishing returns on range.

5. Application to Debris Classes and Benchmark Comparison

The radiometric + SNR framework from Section 4 is applied to debris diameters of 1 cm, 5 cm, and 10 cm. The purpose is to quantify local-volume detectability under bounded integration and realistic sensor noise.

5.1 Sensor Constants (ACUROS6 CQD-CMOS)

- Spectral range: 400–1700 nm
- Quantum efficiency: >20% at 1550 nm; conservative band-effective $QE_e = 0.20$
- Read noise: 20 e^- RMS (high gain), 125 e^- RMS (low gain). High gain used for faint-target operation.
- Well depth: 52 ke^- (high gain), 350 ke^- (low gain)
- Minimum exposure: microsecond-scale; operated at millisecond-scale per smear constraints

5.2 Scenarios and Assumptions

Optics and stacking constants common across all cases: aperture $D_{ap} = 5$ cm ($A_{ap} = 1.96 \times 10^{-3}$ m²), throughput $\tau_{opt} = 0.8$, frame exposure t = 10 ms, N = 50 subframes (T = 0.5 s total), $\sigma_r = 20\ e^-$ RMS (high gain), $n_{pix} = 1$ (track-aligned stacking).

Three explicit regimes are evaluated for each debris size (nine outcomes total). Worst-case (baseline limb): ρ = 0.10, Φ = 60° (F ≈ 0.48), bright Earth-limb background. Median-case (reduced limb): ρ = 0.10, Φ = 45°, reduced limb background. Optimal-case (upper-bound dark sky): ρ = 0.20, Φ = 0° (F ≈ 1), dark-sky/off-limb background. The optimal case is explicitly an upper bound rather than a baseline.

5.3 Signal Anchor Point

Section 4 provides the concrete baseline reference: $N_{e,sig}(R = 5\ km) \approx 254\ e^-$/frame for a 1 cm debris object using $QE_e = 0.30$. Anchoring to ACUROS6-class $QE_e = 0.20$

rescales this to:

$$N_{e,sig}(5\ km) \approx 254 \times (0.20 / 0.30) \approx 169\ e^- / frame$$

For other sizes and ranges, $N_{e,sig} \sim D^2$, $N_{e,sig} \sim 1/R^2$, $N_{e,sig} \sim \rho\ F(\Phi)$.

5.4 Results

Table 1 presents the detectability range matrix (SNR_{min} = 5, 0.5 s stacked) using QE_e = 0.20 [11, 12], N = 50, t = 10 ms, σ_r = 20 e^- RMS, n_{pix} = 1.

Regime	1 cm	5 cm	10 cm
Worst-case (baseline limb)	13 km	66 km	133 km
Median-case (reduced limb)	20 km	98 km	195 km
Optimal-case (upper bound, dark sky)	35 km	175 km	350 km†

† The optimal 10 cm value is an upper-bound sensitivity number. Practical line-of-sight geometry, illumination conditions, and track-coadd feasibility typically become the binding constraint before detector sensitivity at these scales.

The matrix demonstrates expected scaling from the Section 4 model: $N_{e,sig} \sim D^2/R^2$, so R_{max} scales approximately linearly with debris diameter D for fixed noise and stacking strategy. The worst-to-optimal spread is primarily controlled by background regime and $\rho\ F(\Phi)$.

Conclusion

Physics-based detectability bounds have been established for a compact CQD-CMOS optical sensor observing centimeter-scale orbital debris under realistic radiometric and engineering constraints. By explicitly modeling signal formation, background and detector noise, exposure limits, and bounded frame stacking, regimes are identified in which optical detection is physically feasible, with quantified dependence on object size, range, and observing geometry.

The resulting detectability ranges are physics-limited bounds, not guarantees of operational performance. This analysis does not address probability of detection, false-alarm rates, orbit determination accuracy, sky coverage, search strategies, or revisit rates. Variability in illumination geometry, background radiance, pixel footprint growth, and onboard processing assumptions will further limit effective operational range.

These bounds demonstrate that compact CQD-CMOS optical sensors are not suitable for global SSA or comprehensive debris cataloging, particularly for sub-centimeter objects. However, they support a complementary role in local, onboard debris awareness for proximity navigation, where short-range detection of otherwise untracked debris may provide timely situational cues relevant to spacecraft risk

assessment and operational decision-making.

The detectability framework developed here is intended as a foundation for subsequent work, including probabilistic detection modeling, operational performance evaluation, constellation-level coverage analysis, and techno-economic assessment. Together, these extensions will determine how first-principles detectability translates into practical risk reduction and system-level value.

References

[1] NASA Orbital Debris Program Office (ODPO), “Optical Measurements,” NASA Johnson Space Center. [Online]. Available: https://orbitaldebris.jsc.nasa.gov/measurements/optical.html

[2] NASA, “Photometric Observations of Geosynchronous Orbit Debris,” NASA Technical Reports Server, Report No. 20100017871, 2010. [Online]. Available: https://ntrs.nasa.gov/citations/20100017871

[3] NASA, “Observations of Human-Made Debris in Earth Orbit,” NASA Technical Reports Server, Report No. 20110024043, 2011. [Online]. Available: https://ntrs.nasa.gov/api/citations/20110024043/downloads/20110024043.pdf

[4] P. Seitzer et al., “Optical Photometric Studies of GEO Debris,” in Proc. 2009 AMOS Technical Conference, Maui, HI, 2009. [Online]. Available: https://amostech.com/TechnicalPapers/2009/Orbital_Debris/Seitzer.pdf

[5] P. Seitzer et al., “Optical Photometric Observations of GEO Debris,” in Proc. 2010 AMOS Technical Conference, Maui, HI, 2010. [Online]. Available: https://amostech.com/TechnicalPapers/2010/Orbital_Debris/Seitzer.pdf

[6] ASTM International, “ASTM E490-22: Standard Solar Constant and Zero Air Mass Solar Spectral Irradiance Tables,” West Conshohocken, PA, 2022. [Online]. Available: https://www.astm.org/e0490-22.html

[7] Hamamatsu Photonics, “Calculating SNR for Scientific Cameras,” Technical Guide. [Online]. Available: https://camera.hamamatsu.com/jp/en/learn/technical_information/thechnical_guide/calculating_snr.html

[8] Hamamatsu Photonics, “CCD Signal-to-Noise Ratio,” Hamamatsu Learning Center. [Online]. Available: https://hamamatsu.magnet.fsu.edu/articles/ccdsnr.html

[9] Hamamatsu Photonics, “Read Noise,” Technical Guide. [Online]. Available: https://camera.hamamatsu.com/jp/en/learn/technical_information/thechnical_guide/read_noise.html

[10] SWIR Vision Systems, “Acuros Product Documentation,” 2024. [Online]. Available: https://www.swirvisionsystems.com/swir-resources/acuros-product-documentation/

[11] SWIR Vision Systems, “Acuros6 Sensor Product Sheet,” Jan. 2024. [Online]. Available: https://www.swirvisionsystems.com/wp-content/uploads/2024/01/Acuros6-Sensor-ProductSheet_0124.pdf

[12] SWIR Vision Systems, “ACUROS6 SWIR CLINK LBP GEVK-D Data Sheet,” 2025. [Online]. Available: https://www.swirvisionsystems.com/wp-content/uploads/2025/07/ACUROS6-SWIR-CLINK-LBP-GEVK-D.pdf

[13] J. Stuart et al., “SBV/MSX End-of-Life Experiments,” in Proc. 2008 AMOS Technical Conference, Maui, HI, 2008. [Online]. Available: https://amostech.com/TechnicalPapers/2008/SSA_and_SSA_Architecture/Stuart.pdf

[14] M. Miller, “The Space-Based Visible Sensor’s Contribution to Space Catalog Maintenance,” The MITRE Corporation. [Online]. Available: https://www.mitre.org/sites/default/files/pdf/miller_space_based.pdf

[15] J. Scott et al., “SAPHIRE On-Orbit Results,” in Proc. 2013 AMOS Technical Conference, Maui, HI, 2013. [Online]. Available: https://amostech.com/TechnicalPapers/2013/Space-Based_Assets/SCOTT.pdf

[16] Department of Energy, “Sapphire System Performance and Limiting Magnitude,” OSTI Technical Report, 2016. [Online]. Available: https://www.osti.gov/servlets/purl/1253293

[17] M. Shtofenmakher and H. Balakrishnan, “Detection of Small Space Debris Using Commercial Star Trackers,” in Proc. IAA Space Traffic Management Conference, 2023. [Online]. Available: https://www.mit.edu/~hamsa/pubs/ShtofenmakherBalakrishnan-IAA-STM-2023.pdf

[18] Inter-Agency Space Debris Coordination Committee (IADC), “IADC Space Debris Mitigation Guidelines,” Revision 2, 2012. [Online]. Available: https://orbitaldebris.jsc.nasa.gov/library/iadc-space-debris-guidelines-revision-2.pdf

[19] United Nations Office for Outer Space Affairs (UNOOSA), “Compilation of Space Debris Mitigation Standards Applicable to the Design, Operation, and Disposal of Spacecraft,” A/AC.105/C.1/2025/CRP.9, 2025. [Online]. Available: https://www.unoosa.org/res/oosadoc/data/documents/2025/aac_105c_12025crp/aac_105c_12025crp_9_0_html/AC105_C1_2025_CRP09E.pdf

[20] C. Bloom et al., “Space and Ground-Based SDA Sensor Performance Comparisons,” in Proc. 2022 AMOS Technical Conference, Maui, HI, 2022.